

Wind power spectra for coastal area of East Jiangsu Province based on SHMS

Hao Wang^{*1}, Tianyou Tao^{1a} and Teng Wu^{2b}

¹Key Laboratory of C&PC Structures of Ministry of Education, Southeast University, No. 2 Sipailou, Nanjing 210096, China

²Department of Civil, Structural and Environmental Engineering, University at Buffalo, State University of New York, Buffalo, NY 14126, USA

(Received October 1, 2015, Revised January 9, 2016, Accepted January 11, 2016)

Abstract. A wind velocity power spectrum (WVPS) with high fidelity is extremely important for accurate prediction of structural buffeting response. WVPS heavily depends on the geographical locations, local terrains and topographies. Hence, field measurement of wind characteristics may be the unique way to obtain the accurate WVPS for a specific region. In this paper, a systematic analysis and discussions of existing WVPSs were performed. Six recorded strong wind data from the structural health monitoring systems (SHMS) of Runyang Suspension Bridge (RSB) and Sutong Cable-stayed Bridge (SCB) in Jiangsu Province of China were selected for analysis. The measured and pre-processed wind velocity data was first transformed from time domain to frequency domain to obtain the measured spectrum. The spectrum for each strong wind was then fitted using the nonlinear least square method and compared with both the fitted spectrum from statistical analysis and the recommended spectrum in specifications. The modified Kaimal spectrum was proved to be the “best” choice for the coastal area of East Jiangsu Province. Finally, a suitable WVPS formula fit for the coastal area of East Jiangsu Province was presented based on the modified Kaimal spectrum. Results in this study provide a more accurate and reliable WVPS for wind-resistant design of engineering structures in the coastal area of East Jiangsu Province.

Keywords: wind velocity; power spectrum; strong wind; coastal area of East Jiangsu Province; structural health monitoring

1. Introduction

The long-span cable-supported bridges, including cable-stayed bridges and suspension bridges, are distinguished for the excellent spanning capabilities as well as the structural-aesthetic advantages (Gimsing 1983). A large number of long-span cable-supported bridges have been constructed around the world, e.g., the Akashi Kaikyo Bridge (suspension bridge with a main span of 1991 m) in Japan, the Xihoumen Bridge (suspension bridge with a main span of 1650 m) in China, and the Russian Island Bridge (cable-stayed bridge with a main span of 1104 m) in Russia.

*Corresponding author, Professor, E-mail: wanghao1980@seu.edu.cn

^a Ph.D. Candidate, Email: taotianyou@seu.edu.cn

^b Assistant Professor, Email: tengwu@buffalo.edu

With the increase of bridge span, these structures become very flexible due to the rapid decrease of natural frequencies and are very sensitive to wind actions (Xu *et al.* 2000, Chen and Kareem 2002, Wang *et al.* 2013, Huang *et al.* 2014). As a result, the wind loads generally behave as the dominated actions in the design of super-long-span bridges. The aerodynamic performance of long-span cable-supported bridges is therefore needed for special concerns in the design stage.

As the wind characteristics heavily depend on the geographical location, local terrains and topographies, it is important to carefully consider these site-dependent features to achieve the accurate wind-input simulation in the bridge aerodynamics analysis. The wind characteristics mainly include averaged wind features, e.g., mean wind velocity and wind velocity profile, and fluctuating wind characteristics, e.g., turbulence intensity, gust factor, turbulence integral scale, and power spectral density (also called power spectrum). (Simiu and Scanlan 1996, Li *et al.* 2012a, Wang *et al.* 2015). Among them, the power spectrum is a crucial parameter that determines the prediction of wind-induced responses of engineering structures (Kareem 1985, Huang *et al.* 2013, Wu and Kareem 2013). The wind velocity power spectrum (WVPS) statistically represents the energy distribution of a turbulent wind field among a range of scales or frequencies. According to the WVPS, the turbulent wind can be viewed as a superposition of eddies ranging spatially from millimeters to kilometers and temporally from a fraction of a second to hours. In the previous pioneering researches on the winds in the atmospheric boundary layer, a series of empirical wind power spectrum models, such as Davenport Spectrum (Davenport 1961), Kaimal Spectrum (Kaimal 1972), and Karman Spectrum (Von Karman 1948) have been advanced primarily for extratropical strong winds and adopted by several national specifications. However, as indicated in the abovementioned content, the wind spectrum may deviate from the existing empirical models due to the influence of specific geography of each bridge site. Furthermore, for a typhoon/hurricane-prone area, it is necessary to take the wind characteristics of the tropical cyclones into account. The downward transport of convective cells from aloft modulates the typhoon/hurricane near sea surface, and convective turbulence and mesoscale motion may play a prominent role in energy transport at different scales. As a result, the turbulent energy distribution may not exactly reflect the features observed in extratropical wind flows (Li *et al.* 2012b). Currently, all the specifications employ a unified wind spectrum for both extratropical and tropical areas. Hence, it is essential to improve existing spectral models based on both extratropical strong winds and tropical cyclone winds for a specific typhoon/hurricane-prone region.

Actually, there is a very long coastline in the eastern part of China, and rivers are densely distributed in the southeastern region (Wang *et al.* 2009, 2010). Influenced by the local climates, the coastal areas are directly vulnerable to the Pacific typhoons which occur more and more frequently in recent few years. Meanwhile, the development of economics promotes the improvement of existing transportation networks. A series of long-span bridge projects across the Yangtze River and sea-crossing projects have been constructed or still under construction in the wind-prone areas. In such a case, it is necessary to better understand the wind characteristics and obtain the reliable WVPS adapted to the site conditions. Accordingly, some suggestions can be provided to the modification of existing codes and used to guide the wind-resistant design in engineering practices.

In order to fully understand the wind characteristics of a certain area, the most effective and direct approach is to conduct intensive field measurements and statistically extract the target information from accumulated measured data. Since 1970s, some fruitful work has been done on strong wind climates in developed countries. Many wind databases were established to facilitate wind climate researches, for instance, the Sparks database in the USA (Sparks *et al.* 1992), the

Kato database in Japan (Kato *et al.* 1992), and the Froya database in Norway (Andersen and Lovseth 1995). However, most of them are used for meteorological applications and cannot be directed used in the wind-resistant design of engineering structures. Recently, the rapid development of structural health monitoring provides another promising approach for the site monitoring of wind characteristics (Xu *et al.* 2000, Li *et al.* 2004a, b, Wang *et al.* 2015). Structural health monitoring is realized by an integrated intelligent system called structural health monitoring system (SHMS). To date, many SHMSs have been proposed and successfully implemented on full-scale bridges, e.g., Tsing Ma Bridge in China (Xu *et al.* 2000) and Jindo Bridge in Korea (Jang *et al.* 2010). Anemometers are usually included in the SHMSs of long-span flexible bridges to monitor the wind environment at the bridge site, offering the potential for the investigation of strong wind characteristics and the accumulation of site wind databases (Chen *et al.* 2002, Cho *et al.* 2010). With the aid of SHMS, a great number of researches on the wind characteristics in the coastal area of China have been conducted (Xu *et al.* 2000, Liu *et al.* 2009, Zhao *et al.* 2009, Hui *et al.* 2009a, b, Wang *et al.* 2010, Li *et al.* 2012a). On the other hand, the coastal line of China is so long that existing research achievements cannot satisfy with each region along the coastal line. Hence, more field measurements on strong wind characteristics are needed for each region in the eastern part of China.

As RSB and SCB in Jiangsu Province are two important national projects in China, structural health monitoring systems have been successfully installed on these two bridges, offering the opportunities to collect precious real-time data during strong winds and typhoons in the coastal area of East Jiangsu Province. In this paper, the WVPS for the coastal area of East Jiangsu Province is investigated. Several strong wind and typhoon records acquired at RSB site and SCB site are taken as the research wind samples. Accordingly, a new wind spectrum adapted to east coastal areas of Jiangsu Province in China is presented. The new spectrum can provide references for wind-resistant design of engineering structures in this area.

2. Engineering background

The locations of RSB and SCB are shown in Fig. 1. The two bridges are both located in the eastern part of the Asian continent where the weather is dominated by the humid subtropical monsoon climate. In this area, the thermal difference between sea and land promotes obvious seasonal wind climates, e.g., strong northern wind from Siberia in winter and strong eastern wind from the Pacific Ocean in summer. Additionally, typhoon is an extreme wind event that is frequently encountered in each summer at the coastal area of Eastern Jiangsu Province. Since the long-span bridges are sensitive to the wind actions due to the inherent flexible features, the wind characteristics around the bridges should be specially monitored in such a wind-prone area.

2.1 Runyang suspension bridge

RSB is a steel-box-girder suspension bridge with a main span of 1490 m. When it was open to traffic in 2005, it was the longest suspension bridge in China and the third in the world. The overall layout is shown in Fig. 2. In RSB, the sag-to-span ratio is 1:9.96, and the two side spans are both 470 m long. The main span is separated from the side spans with the expansion joints at the main towers.



Fig. 1 Locations of RSB and SCB

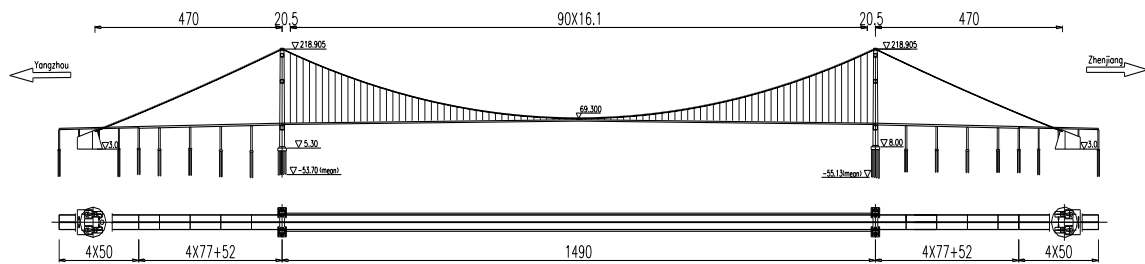


Fig. 2 Elevation layout of RSB (Unit: m)

The fully welded flat streamlined steel box girder is employed in RSB. The girder is 1485.16 m long and simply supported by the two towers. The tower is a reinforced concrete multi-storey portal frame. The pylons are 210 m in height and are rectangular single-chamber structures with variable wall thickness. The main cables are made of prefabricated parallel strands with a distance of 34.4 m between each other. 91 pairs of suspenders are adopted to connect the main cables and the main girder, while a pair of central buckle is installed at the midspan. Two gravity-type concrete anchorages are assigned to each side to neutralize the tensile forces from the main cables.

2.2 Sutong cable-stayed bridge

SCB, located between Suzhou and Nantong, is a two-tower twin-cable-plane, steel-box-girder cable-stayed bridge with a main span of 1088 m. When it was open to traffic in 2008, it was the first longest cable-stayed bridge in the world and a record-breaking project in cable-stayed bridges. At that time, the bridge had three other No.1s in the world including the main tower height of 306 m, the cable-stayed length of 580 m, and the group pile foundation's plane size of 113.75 m × 48.1 m. SCB is one of the largest bridge projects in the bridge history of China. The overall structural arrangement of SCB is shown in Fig. 3.

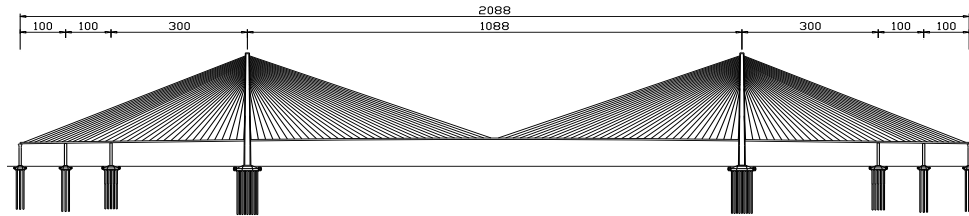


Fig. 3 Elevation layout of SCB (Unit: m)

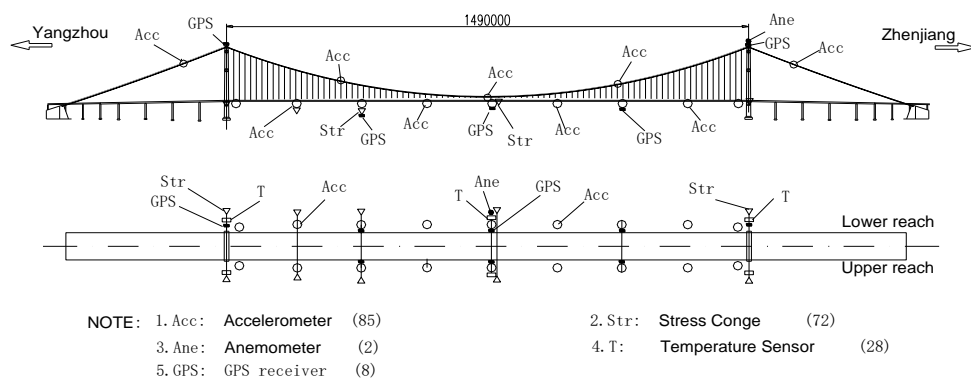


Fig. 4 Sensors layout in the SHMS of RSB

3. Wind data source

3.1 SHMSs of the two bridges

The SHMS of RSB, as shown in Fig. 4, adopts two WA15 anemometers by Finnish company, Vaisala, installed in the middle of the main span (69.3 m high) and on top of the southern tower (218.9 m high). The anemometers are installed towards due north. The wind angle of the true northern wind is defined as zero degree and the angles in the clockwise direction is measured as positive, so that due east is naturally measured as 90 degrees. The working temperature of the anemometers is -50~55°C and the measurement accuracy is less than 0.1 m/s. Considering the daily storage amount of the hard disks, the sampling frequency is set as 1 Hz and their recorded data includes the wind velocity V and the azimuth β . Ten years of usage and analytical results from related researches have shown that the anemometer has a high working stability and good dynamic tracking performance, and is capable of acquiring accurate and reliable data.

In the SHMS of SCB, as shown in Fig. 5, there are four anemometers available for the monitoring of wind environment. Two of them are installed on top of the southern and northern towers, respectively. And the others are separately installed on the upper-stream side and lower-stream side of the midspan. The anemometers are three-axis ultrasonic anemometers produced by the Delta OHM Company, Italy. The wind velocity ranging from 0~60 m/s can be accurately recorded with a resolution of 0.01 m/s. The azimuth measurement can successfully

record the wind directions from 0° to 359.9° with a resolution of 0.1°. In the temperature ranging from -40°C to 60°C, the anemometers can work well with stable and accurate wind data recorded. Other parameters are kept the same as those of anemometers on RSB.

3.2 Field measurements

In addition to the wind data from SHMSs, more field measurements at RSB and SCB sites were performed, where the 1590-PK-020 3D ultrasonic anemometer produced by the Gill Instruments Ltd. is adopted, as shown in Fig. 6(a). In order to record the wind data correctly, the anemometer was installed at the windward side in the middle of the main span to reduce the influence by the bridge. The instrument provides high sampling frequency, high precision, and stable and reliable data acquisition and storage. The sampling frequency is set as 20 Hz in this study. Fig. 6(b) shows the adjustment of the measurement instruments.

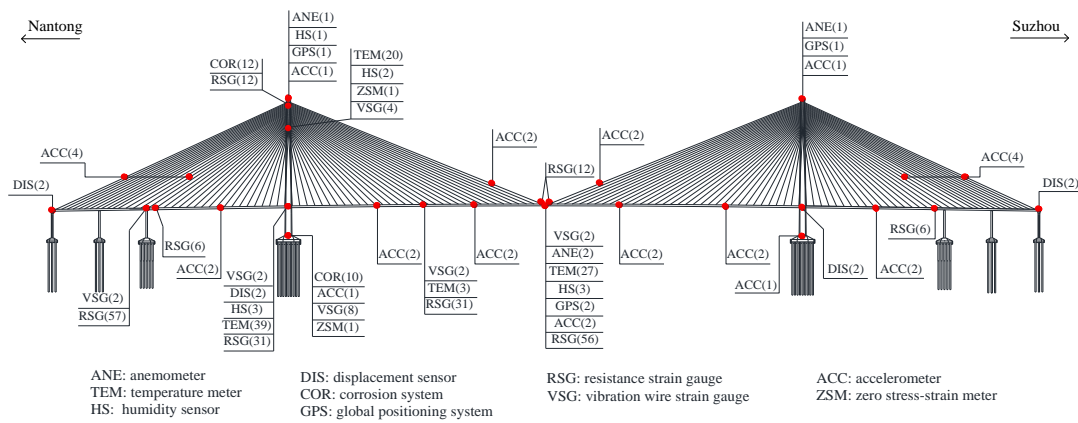


Fig. 5 Sensors layout in the SHMS of SCB



(a) 3D ultrasonic anemometer

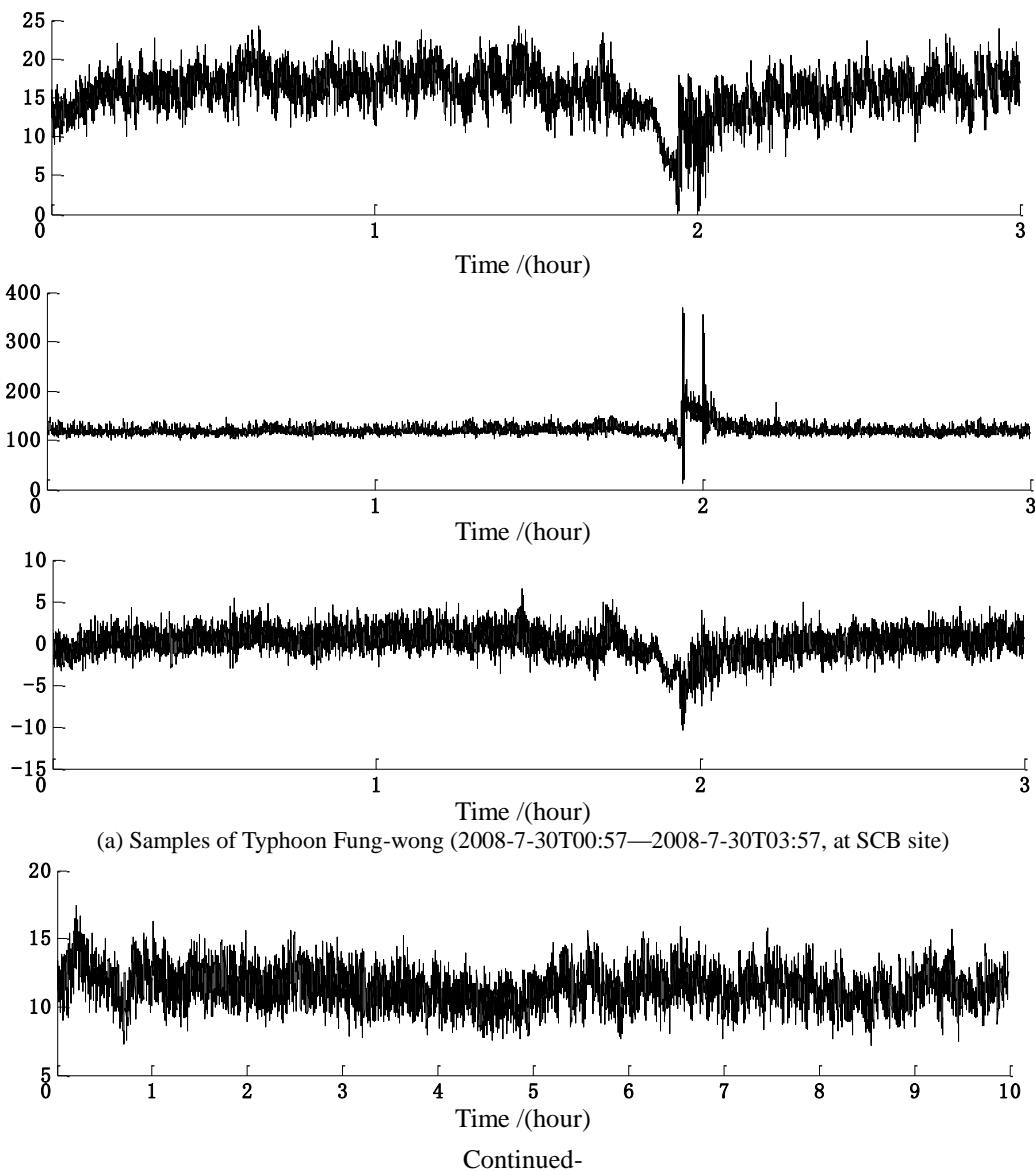


(b) Adjusting the measurement instruments

Fig. 6 Photos of field measurements during strong winds

3.3 Measured strong wind samples

Intensive wind data have been accumulated at RSB and SCB sites during typhoons and extratropical strong winds based on the SHMSs and field measurements (Wang *et al.* 2009, 2010). In this paper, six typical strong wind records including Typhoon Khanun and Masta in 2005, Wipha in 2007, Kalmaegi and Fung-wong in 2008, and Strong Northern Wind are selected for the following spectral analyses. Considering the significant reference values of the measured wind data, Fig. 7 presents three typical samples of Typhoon Fung-wong, Typhoon Kalmaegi and strong northern wind.



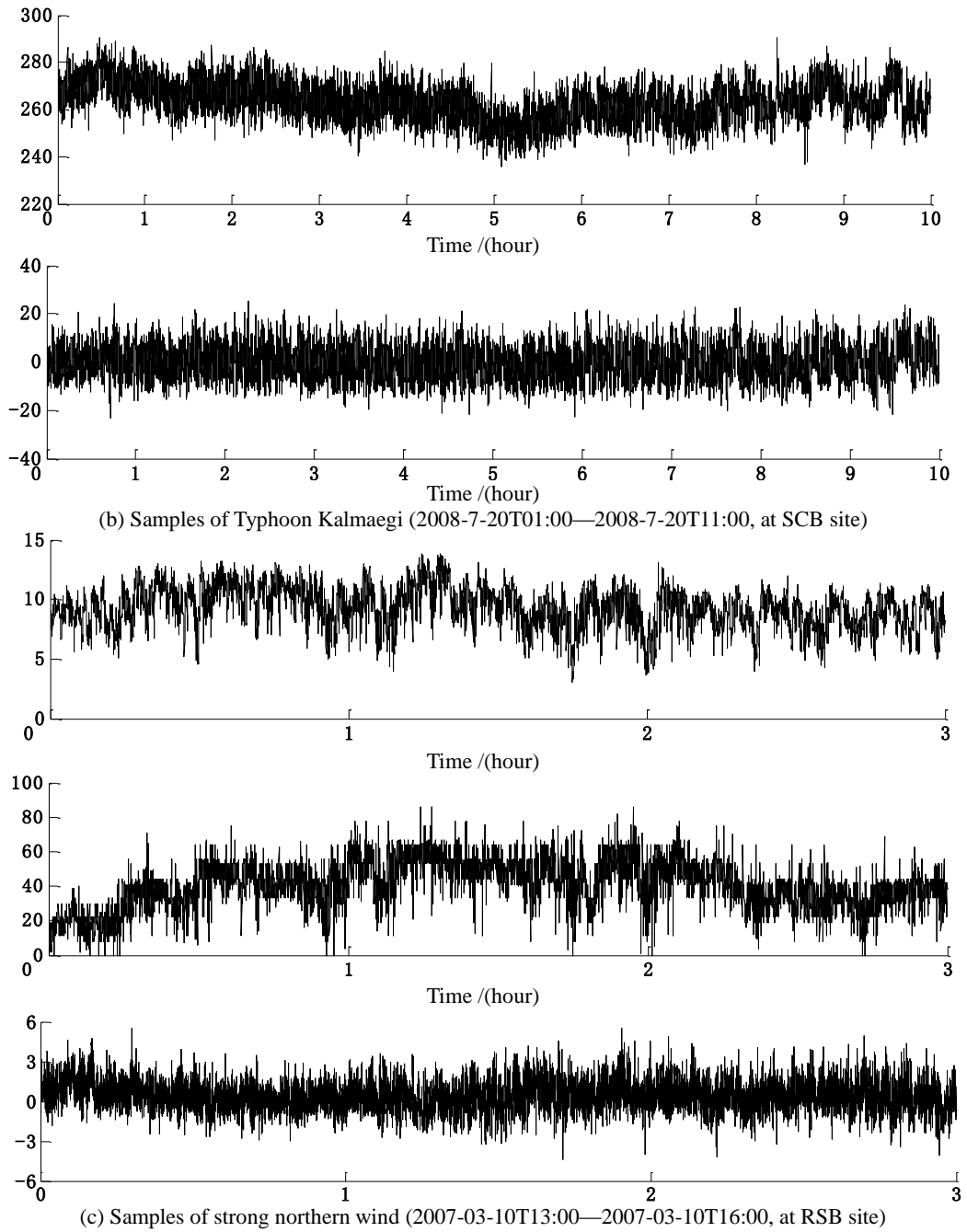


Fig. 7 Measured strong wind data samples

4. Formulas of WVPS

The study on WVPS of atmospheric boundary layer winds has been a crucial issue in structural

wind engineering. Some pioneering work has been well documented by the scientists such as Von Karman (1948), Davenport (1961), and Simiu and Scanlan (1996). Several useful formulas of WVPS for along-wind, cross-wind and vertical turbulence were introduced based long-term field measurements (e.g., Von Karman 1948, Kaimal 1972, Harris 1970, Panofsky and Dutton 1984, Simiu and Scanlan 1996). In the bridge buffeting analysis, only along-wind and vertical WVPS are concerned, so the following presentation and analysis mainly focus on these two cases.

4.1 Along-wind WVPS

4.1.1 Von Karman spectrum

$$\frac{n \cdot S_u(z, n)}{u_*^2} = \frac{4\beta x}{(1 + 70.8x^2)^{5/6}}, \quad x = \frac{nL_u^x}{U(z)} \quad (1)$$

where $S_u(z, n)$ is the power spectrum of along-wind turbulence; n is the natural frequency of turbulence; $U(z)$ is the mean wind velocity at the height of z m; L_u^x is the along-wind turbulence integral scale; u_* is the friction wind velocity; β is the coefficient of friction wind velocity. u_* and β have a relationship that can be described as $\sigma_u^2 = \beta u_*^2$; and σ_u is the standard deviation of along-wind turbulence.

4.1.2 Davenport spectrum

$$\frac{n \cdot S_u(z, n)}{u_*^2} = \frac{4.0x^2}{(1 + x^2)^{4/3}}, \quad x = \frac{1200n}{U(10)} \quad (2)$$

where $U(10)$ = the mean wind velocity at the height of 10 m.

Davenport spectrum has been adopted by NBCC (National Building Code of Canada, 1970) and ANSI (American National Standards Institute, 1972). It is clear that this spectrum is independent from the altitude. However, its comparison with measured spectra at Sale, Australia indicates that this formula may cause an overestimation as much as 100-400% to the high-frequency region of the real site WVPS (Simiu and Scanlan 1996).

4.1.3 Kaimal spectrum

$$\frac{n \cdot S_u(z, n)}{u_*^2} = \frac{200x}{(1 + 50x)^{5/3}}, \quad x = \frac{zn}{U(z)} \quad (3)$$

This spectrum is adopted by the wind-resistant design specification for highway bridges in China (2004). It has been frequently used in the modeling of wind field, buffeting analysis of long-span bridges as well as turbulence verification in wind tunnel tests.

4.1.4 Harris spectrum

$$\frac{nS_u(z, n)}{u_*^2} = \frac{2x}{3(2 + x^2)^{5/6}}, \quad x = \frac{1800n}{U} \quad (4)$$

Harris spectrum takes a value of 1800 instead of the altitude or turbulence integral scale in the Moning coordinate, while the influence of altitude is included in the mean wind velocity. Hence, unlike Davenport spectrum, Harris spectrum is not a spectrum that is fully irrelevant to the

altitude.

4.2 Vertical WVPS

Since many employed anemometers are two dimensional and therefore few measured wind data of vertical fluctuations are available, very limited researches were concentrated on vertical WVPS comparing to the along-wind WVPS. Hence, only two classical models of vertical turbulence, i.e., Panofsky spectrum and Lumley-Panofsky spectrum, are presented.

4.2.1 Panofsky spectrum

$$\frac{nS_w(z, n)}{u_*^2} = \frac{6x}{(1+4x)^2}, \quad x = \frac{zn}{U(z)} \quad (5)$$

4.2.2 Lumley-panofsky spectrum

$$\frac{nS_w(z, n)}{u_*^2} = \frac{3.36x}{1+10x^{5/3}}, \quad x = \frac{zn}{U(z)} \quad (6)$$

5. Regression analysis of WVPS

All the wind data utilized in the spectral analysis were pre-processed. Each record was first normalized to the same altitude with the commonly used power law (Kareem 1985). Then, the vector decomposition of wind velocity considering wind direction and attack angle was carried out. The obtained along-wind and vertical turbulences were transformed from time domain to frequency domain to acquire the WVPS of each record using Welch transformation (The MathWorks Inc. 2010). Finally, the nonlinear least-square method was selected for the regression analysis of the measured WVPS based on prescribed mathematical expressions of the wind spectra.

5.1 Along-wind WVPS

The nonlinear regression analysis of the six strong winds using five different WVPS formulas are conducted, and the analytic expressions of fitted spectra are shown in Tables 1-6. It should be noted that Karman, Davenport, Kaimal and Harris in spectrum column in Tables 1-6 refer to the fitted spectrum that takes the prescribed mathematical expressions corresponding to models in Eqs. (1)-(4), respectively. For example, the Karman WVPS density function is the fitted spectrum based on the model of $[a_1\beta x/(1+a_2x^2)^{5/6}]$ in the regression analysis, where a_1 and a_2 are parameters to be determined. This indicates only the scale coefficients before the Monin coordinate x are taken as undetermined parameters while the other parameters are kept unchanged. In order to quantify the difference between the measured spectrum and each fitted spectrum, the corresponding root-mean-square errors (RMSE) are also presented in Tables 1-6. The RMSE can be calculated as Eq. (7).

$$RMSE = \sqrt{\frac{1}{n} \sum_{i=1}^n di^2} \tag{7}$$

where di is the deviation between the measured and fitted spectra at each frequency; n is the number of discrete frequencies.

It should be mentioned that only the relatively stationary wind data of 0.5~2 hours is selected for the spectral estimation. Tables 1-6 show that, generally minimum RMSE value is obtained when the Kaimal spectrum is selected as the target spectrum. Hence, a modified Kaimal formula is further proposed as following

$$\frac{n \cdot S_u(z, n)}{u_*^2} = \frac{ax}{(1 + bx^c)^{5/3c}} \tag{8}$$

where a, b, c are coefficients that need to be determined. It is noted that, for the modified Kaimal spectrum, the exponent of the Monin coordinate x in the denominator and the exponent of the denominator are also taken as undetermined parameters. These two parameters depend on each other so that the Kolmogrov hypothesis is satisfied in the obtained modified Kaimal spectrum (Simiu and Scanlan 1996). The fitted results based on the modified Kaimal formula are also presented in Tables 1-6.

Table 1 Regression results of Khanun

Spectrum	WVPS density function	RMSE
Karman	$\frac{0.78 \cdot \beta \cdot x}{(1 + 5.22 \cdot x^2)^{5/6}}$	0.1476
Davenport	$\frac{4.63 \cdot x^2}{(5.58 + x^2)^{4/3}}$	0.1561
Kaimal	$\frac{36.15 \cdot x}{(1 + 10.69 \cdot x)^{5/3}}$	0.1464
Harris	$\frac{6.21 \cdot x}{(27.23 + x^2)^{5/6}}$	0.1467
Modified Kaimal	$\frac{21.18 \cdot x}{(1 + 16.34 \cdot x^{(1/0.75)})^{5 \cdot 0.75/3}}$	0.1448

Table 2 Regression results of Masta

Spectrum	WVPS density function	RMSE
Karman	$\frac{1.08 \cdot \beta \cdot x}{(1 + 7.03 \cdot x^2)^{5/6}}$	0.2232
Davenport	$\frac{4.85 \cdot x^2}{(3.46 + x^2)^{4/3}}$	0.2332
Kaimal	$\frac{40.3 \cdot x}{(1 + 10.55 \cdot x)^{5/3}}$	0.1950
Harris	$\frac{6.67 \cdot x}{(20.17 + x^2)^{5/6}}$	0.2232
Modified Kaimal	$\frac{246.7 \cdot x}{(1 + 5.40 \cdot x^{(1/1.90)})^{5 \cdot 1.90/3}}$	0.1847

Table 3 Regression results of Kalmaegi

Spectrum	WVPS density function	RMSE
Karman	$\frac{6.69 \cdot \beta \cdot x}{(1 + 263.8 \cdot x^2)^{5/6}}$	0.1797
Davenport	$\frac{1.46 \cdot x^2}{(0.087 + x^2)^{4/3}}$	0.1848
Kaimal	$\frac{220.4 \cdot x}{(1 + 58.73 \cdot x)^{5/3}}$	0.1634
Harris	$\frac{2.01 \cdot x}{(0.54 + x^2)^{5/6}}$	0.1797
Modified Kaimal	$\frac{236.7 \cdot x}{(1 + 9.16 \cdot x^{(1/1.62)})^{5.62/3}}$	0.1487

Table 4 Regression results of Fung-wong

Spectrum	WVPS density function	RMSE
Karman	$\frac{0.00039 \cdot \beta \cdot x}{(1 + 0.00011 \cdot x^2)^{5/6}}$	0.1735
Davenport	$\frac{1.76 \cdot x^2}{(1.00 + x^2)^{4/3}}$	0.1930
Kaimal	$\frac{0.010 \cdot x}{(1 + 0.027 \cdot x)^{5/3}}$	0.1725
Harris	$\frac{3.72 \cdot x}{(300 + x^2)^{5/6}}$	0.1898
Modified Kaimal	$\frac{1312 \cdot x}{(1 + 1.32 \cdot x^{(1/6.66)})^{5.666/3}}$	0.1725

Table 5 Regression results of Wipha

Spectrum	WVPS density function	RMSE
Karman	$\frac{0.011 \cdot x}{(1 + 0.0098 \cdot x^2)^{5/6}}$	0.1370
Davenport	$\frac{12.59 \cdot x^2}{(3026 + x^2)^{4/3}}$	0.1400
Kaimal	$\frac{0.49 \cdot x}{(1 + 0.43 \cdot x)^{5/3}}$	0.1327
Harris	$\frac{15.87 \cdot x}{(9009 + x^2)^{5/6}}$	0.1382
Modified Kaimal	$\frac{1.04 \cdot x}{(1 + 0.71 \cdot x^{(1/1.33)})^{5.33/3}}$	0.1325

Table 6 Regression results of Northern Wind

Spectrum	WVPS density function	RMSE
Karman	$\frac{2.98 \cdot x}{(1 + 36.52 \cdot x^2)^{5/6}}$	0.1705
Davenport	$\frac{3.46 \cdot x^2}{(0.74 + x^2)^{4/3}}$	0.1751
Kaimal	$\frac{124.2 \cdot x}{(1 + 26.61 \cdot x)^{5/3}}$	0.1641
Harris	$\frac{4.66 \cdot x}{(3.89 + x^2)^{5/6}}$	0.1705
Modified Kaimal	$\frac{110.9 \cdot x}{(1 + 30.44 \cdot x^{(1/0.94)})^{5 \cdot 0.94/3}}$	0.1641

Since the modified Kaimal spectrum performs the best in the comparison with measured spectrum, a further regression analysis is conducted based on the six modified Kaimal WVPS density functions, which is similar to the studies conducted by Yu *et al.* (2008). Then a unified WVPS model adapted to the coastal area of East Jiangsu Province is finally obtained, which is detailed as

$$\frac{n \cdot S_u(z, n)}{u_*^2} = \frac{495.4 \cdot x}{(1 + 5.54 \cdot x^{1/2.12})^{5.2.12/3}} \quad (9)$$

As shown in Fig. 8, the unified spectral model for East Jiangsu Province is compared with the measured spectrum of each strong wind record. Also, the Kaimal spectrum and the fitted Kaimal spectra in Tables 1-6 are plotted in Fig. 8 for comparison. The following findings can be drawn.

(1) Most of the measured WVPS of the six strong wind records cannot well satisfy with the Kaimal spectrum. The value of measured spectrum is generally lower in low-frequency and higher in high-frequency regions comparing to the Kaimal spectrum.

(2) An important feature of the measured along-wind WVPS in this study, different from the observations reported by other scholars (e.g., Kareem 1985, Yu *et al.* 2008), is that it presents inflection points as indicated in Typhoon Kalmaegi, Fung-wong and strong northern wind. However, there is no inflection point in existing spectral models. Hence, new spectral expressions should be proposed to consider this observed feature.

(3) The proposed spectrum for East Jiangsu Province can fit the measured results much better than Kaimal spectrum. However, there are still some discrepancies owing to the differences of the six WVPSs and the intrinsic limitations of the modified Kaimal spectrum.

5.2 Vertical WVPS

According to the Wind-Resistant Design Specification for Highway Bridges in China (2004), the Panofsky spectrum is recommended for the vertical WVPS. Here, the prescribed mathematical expression used for regression analysis for the measured vertical turbulence is based on this spectrum. The analysis is similar to that of the along-wind WVPS, and the regression results are shown in Table 7. The fitted Panofsky spectrum versus measured spectrum and Panofsky spectrum is plotted in Fig. 9. Since the anemometers used for measuring Khanun and Masta are two dimensional, the vertical WVPS analyses were performed just for the other four records.

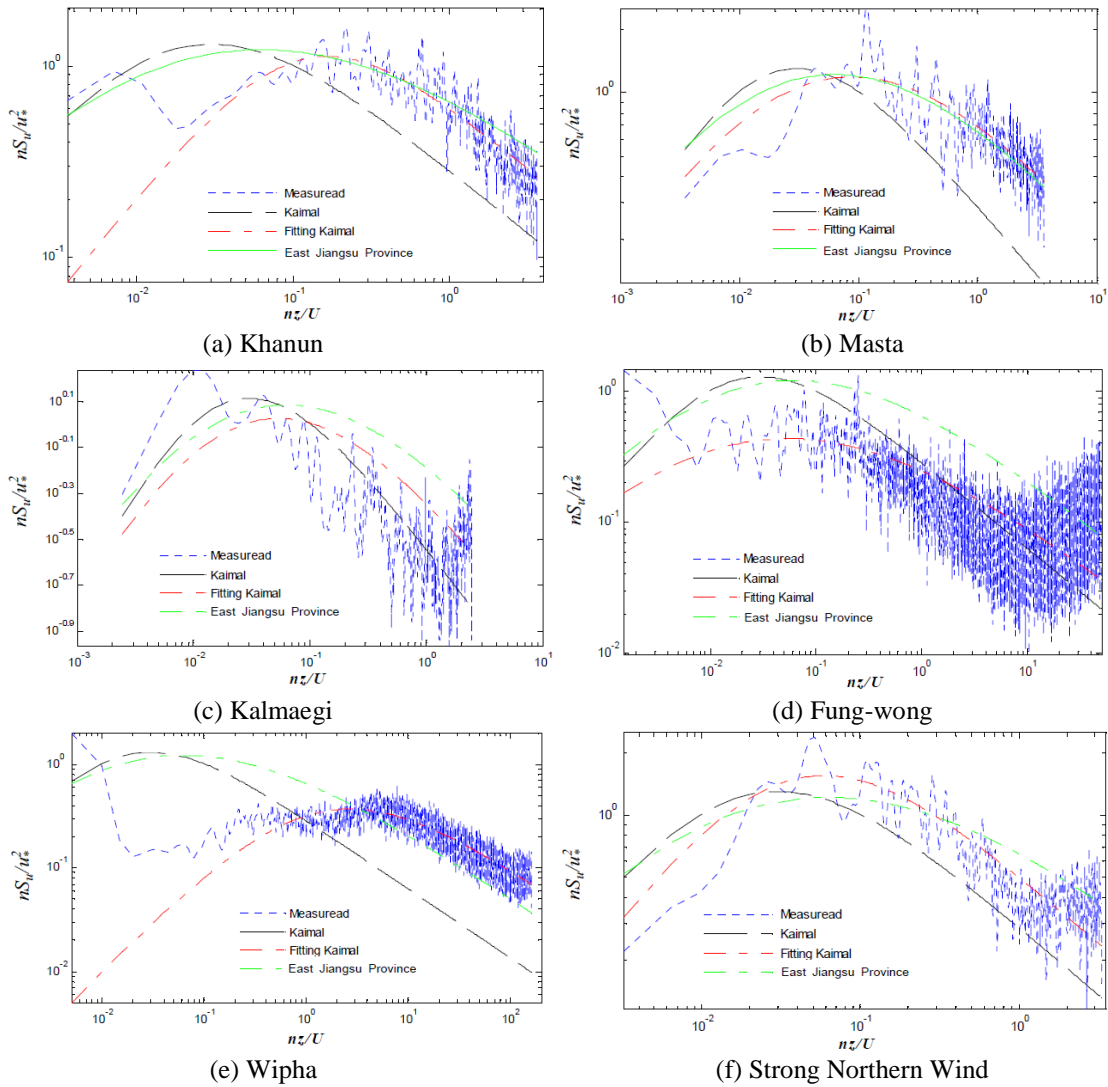


Fig. 8 Comparative analysis on the along-wind WVPS

Table 7 Regression results of vertical turbulence

Wind Event	Fitted Panofsky Spectrum	RMSE
Kalmaegi	$\frac{191.6x}{(1+25.93x)^2}$	0.1875
Fung-wong	$\frac{16x}{(1+2x)^2}$	0.2275
Wipha	$\frac{6.5x}{(1+1.51x)^2}$	0.2383
Strong Northern Wind	$\frac{100.4x}{(1+13.53x)^2}$	0.1970

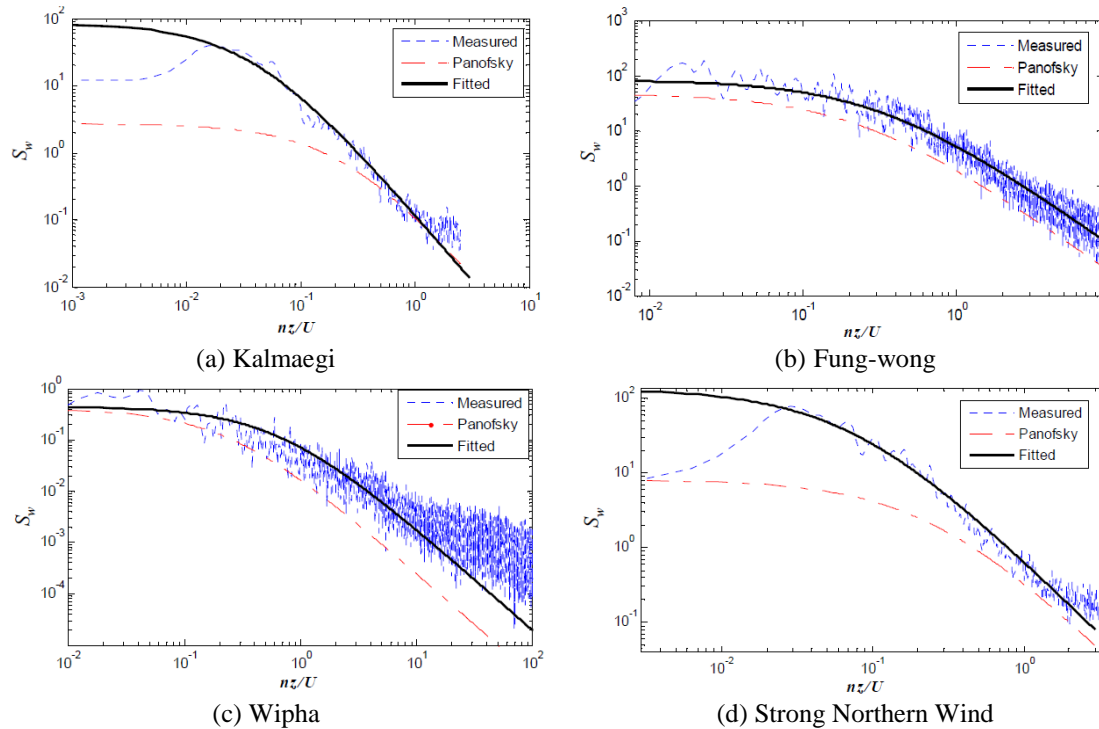


Fig. 9 Comparative analysis on the vertical WVPS

It is obvious that Panofsky spectrum cannot fit well with the measured vertical WVPS, and the value of Panofsky spectrum is generally lower than the measured cases in all frequency bands. On the other hand, the fitted Panofsky spectrum presents the perfect fitness for Typhoon Fung-wong case. For other three cases, it cannot satisfy with the measured spectrum in some frequency ranges. As a result, the Panofsky spectrum may not be an appropriate selection as the prescribed mathematical expression for the spectral regression analysis of vertical turbulence. Due to the aforementioned discrepancies and shortcomings, the vertical WVPS for coastal area of East Jiangsu Province is not proposed in this study.

6. Conclusions

In this paper, the WVPS for the coastal area of East Jiangsu Province in China is analyzed based on the measured strong wind records. The following conclusions can be drawn.

(1) The Kaimal spectrum currently adopted by the Wind-Resistant Design Specification for Highway Bridges in China cannot fit well with the measured along-wind WVPS. Compared with the measured spectrum, the value of Kaimal spectrum is higher in low-frequency and lower in high-frequency bands.

(2) The inflection point is captured in the measured along-wind WVPSs of Typhoon Kalmaegi, Fung-wong and strong northern wind. However, there is no inflection point in the existing spectral

models. Hence, new spectral expressions should be proposed to consider this observed feature.

(3) Compared with other commonly used WVPS models, the minimum RMSE value can be obtained when the modified Kaimal spectrum is adopted as the target spectrum, indicating that the modified Kaimal spectrum is the most appropriate for the derivation of empirical along-wind WVPS of East Jiangsu Province.

(4) According to the six modified Kaimal spectra derived from six strong wind records, a unified WVPS for the coastal area of East Jiangsu Province is proposed. It is obvious that the unified wind spectrum is more suitable than Kaimal to describe the spectral characteristics of strong winds for both typhoon events and strong northern winds.

(5) Panofsky spectrum, whose value is below the measured cases in all frequency bands, cannot fit well with the measured vertical WVPS. Although the fitted Panofsky spectrum presents the perfect fitness for Typhoon Fung-wong case, it cannot satisfy with the measured spectrum in some frequency ranges for other cases. As a result, the Panofsky spectrum may not be an appropriate selection as the prescribed mathematical expression for the spectral regression analysis of vertical turbulence.

It should be noted that only six strong wind records including five typhoons and one monsoon wind are utilized in the analysis. As the wind data accumulated with the time, the regional wind database will be enriched and the unified WVPS will be further improved.

Acknowledgments

The authors would like to gratefully acknowledge the supports from the National Basic Research Program of China (973 Program) (Grant No. 2015CB060000), the National Science Foundation of China (Grant Nos. 51378111 and 51438002), the Fok Ying-Tong Education Foundation for Young Teachers in the Higher Education Institutions of China (Grant No. 142007), the Program for New Century Excellent Talents in University of Ministry of Education of China (Grant No. NCET-13-0128) and the Project Funded by the Priority Academic Program Development of Jiangsu Higher Education Institutions (No. CE02-2-15).

References

- American National Standards Institute. (1972), *American national standard building code requirements for minimum design loads in buildings and other structures*, New York.
- Andersen, O.J. and Lovseth, J. (1995), "Gale force maritime wind, the Froya data base, Part 1: sites and instrumentation, review of the database", *J. Wind Eng. Ind. Aerod.*, **57**(1), 97-109.
- Associate Committee on the National Building Code and National Research Council of Canada. (1970), *Canadian structural design manual*, Ottawa.
- Chen, X.Z. and Kareem, A. (2002), "Advances in modeling of aerodynamic forces on bridge decks", *J. Eng. Mech.- ASCE*, **128**(11), 1193-1205.
- Chen, Z.Q., Wang, X.Y., Ni, Y.Q. and Ko J.M. (2002), "Field measurements on wind-rain-induced vibration of bridge cables with and without MR damper", *Proceedings of the 3rd World Conference on Structural Control*. Como, Italy, January.
- Cho, S., Jang, S.A., Jo, H., Park, J.W., Jung, H.J., Yun, C.B., Spencer, Jr., B.F. and Seo, J.W. (2010), "Structural health monitoring of a cable-stayed bridge using smart sensor technology: data analyses", *Smart Struct. Syst.*, **6**(5-6), 461-480.

- Davenport, A.G. (1961), "The Spectrum of Horizontal Gushiness near the Ground in High Winds", *Q. J. Roy. Meteor. Soc.*, **87**, 194-211.
- Gimsing, N.J. (1983), *Cable-supported bridges: concept and design*, John Wiley & Sons, New York, NY, USA.
- Harris, R.I. (1970), "The nature of the wind", *Proceedings of the Seminar on the Modern Design of Wind Sensitive Structures*, London, UK.
- Huang G.Q., Chen X.Z., Liao H.L. and Li, M.S. (2013), "Predicting of tall building response to non-stationary winds using multiple wind speed samples", *Wind Struct.*, **17**(2), 227-244.
- Huang, D.M, Zhu, L.D. and Chen, W. (2014), "Power spectra of wind forces on a high-rise building with section varying along height", *Wind Struct.*, **18**(3), 295-320.
- Hui, M.C., Larsen, A. and Xiang, H.F. (2009a), "Wind turbulence characteristics study at the Stonecutters Bridge site: Part I – Mean wind and turbulence intensities", *J. Wind Eng. Ind. Aerod.*, **97**(1), 22-36.
- Hui, M.C., Larsen, A. and Xiang, H.F. (2009b), "Wind turbulence characteristics study at the Stonecutters Bridge site: Part II – Wind power spectra, integral length scales and coherences", *J. Wind Eng. Ind. Aerod.*, **97**(1), 48-59.
- Jang, S., Jo, H., Cho, S., Mechitov, K., Rice, J.A., Sim, S.H., Jung, H.J., Yun, C.B., Spencer, Jr. B.F. and Agha, G. (2010), "Structural health monitoring of a cable-stayed bridge using smart sensor technology: deployment and evaluation", *Smart Struct. Syst.*, **6**(5-6), 439-459.
- Kaimal, J.C. (1972), "Spectral Characteristics of Surface Layer Turbulence", *Q. J. Roy. Meteor. Soc.*, **98**, 563-589.
- Kareem, A. (1985), "Wind-induced Response Analysis of Tension Leg Platforms", *J. Struct. Eng.- ASCE*, **111**(1), 37-55.
- Kato, N., Ohukuma, T., Kim, J.R. *et al.* (1992), "Full scale measurements of wind velocity in two urban areas using an ultrasonic anemometer", *J. Wind Eng. Ind. Aerod.*, **41**(1-3), 67-78.
- Li, Q.S., Wu, J.R., Liang, S.G., Xiao, Y.Q. and Wong, C.K. (2004b), "Full-scale measurements and numerical evaluation of wind-induced vibration of a 63-story reinforced concrete super tall building", *Eng. Struct.*, **26**(12), 1779-1794.
- Li, Q.S., Xiao, Y.Q., Wong, C.K. and Jeary, A.P. (2004a), "Field measurements of typhoon effects on a super tall building", *Eng. Struct.*, **26**(2), 233-244.
- Li, L.X., Kareem, A., Xiao, Y.Q. *et al.* (2012a), "Wind profile and spectra in typhoon-prone regions in South China", *Advances in Hurricane Engineering: Learning from Our Past*, USA, Florida, October.
- Li, L.X., Xiao, Y.Q., Kareem, A. *et al.* (2012b), "Modeling typhoon wind power spectra near sea surface based on measurements in the South China sea", *J. Wind Eng. Ind. Aerod.*, **104-106**, 565-576.
- Liu, M., Liao, H.L., Li, M.S. and Ma, C.M. (2009), "Field Measurements of Natural Wind Characteristics at Xihoumen Bridge", *Proceedings of the 2nd International Conference on Transportation Engineering*, Chengdu, China, July.
- Ministry of Communications of PRC. (2004), *Wind-resistant Design Specification for Highway Bridges*. China Communications Press, Beijing, China. (in Chinese).
- Panofsky, H.A. and Dutton. J.A. (1984), *Atmospheric Turbulence: Models and Methods for Engineering Applications*, Wiley, New York, NY, USA.
- Simiu, E. and Scanlan, R.H. (1996), *Wind effects on structures: fundamentals and applications to design*. John Wiley & Sons, INC., New York, NY, USA.
- Sparks, P.R., Reid, G.T. and Reid, E.D. (1992), "Wind conditions in hurricane Hugo by measurement, inference, and experience", *J. Wind Eng. Ind. Aerod.*, **41-44**, 55-66.
- The MathWorks Inc. (2010), *MATLAB & SIMULINK Release Notes for R2010b*, Natick, MA, USA.
- Von Karman, T. (1948), "Progress in the Structural Theory of Turbulence", *Proceedings of the National Academy of Science*, Washington, D. C.
- Wang, H., Hu, R.M., Xie J. *et al.* (2013), "Comparative study on buffeting performance of Sutong Bridge based on design and measured spectrum", *J. Bridge Eng - ASCE*, **18**(7), 587-600.
- Wang, H., Li, A.Q., Guo, T. and Xie, J (2009), "Field measurement on wind characteristic and buffeting response of the Runyang Suspension Bridge during typhoon Matsa", *Sci. China Technol. Sc.*, **52**(2),

1354-1362.

- Wang, H., Li, A.Q. and Jiao, C.K. (2010), "Characteristics of strong winds at the Runyang Suspension Bridge based on field tests from 2005 to 2008", *J. Zhejiang Univ. Sci. A*, **11**(7), 465-476.
- Wang, H., Tao, T.Y., Wu T., Mao, J. and Li, A. (2015), "Joint distribution of wind speed and direction in the context of field measurement", *Wind Struct.*, **20**(5), 701-718.
- Wu, T. and Kareem, A. (2013), "Bridge aerodynamics and aeroelasticity: a comparison of modeling schemes", *J. Fluid Struct.*, **43**, 347-370.
- Xu, Y.L., Zhu, L.D. and Wong, K.Y. (2000), "Field measurement results of Tsing Ma Suspension Bridge during Typhoon Victor", *Struct. Eng. Mech.*, **10**(6), 545-559.
- Yu, B., Chowdhury, A.G. and Masters, F.J. (2008), "Hurricane wind power spectra, cospectra, and integral length scales", *Bound-Lay Meteorol.*, **129**, 411-430.
- Zhao, L., Zhu, L.D. and Ge, Y.J. (2009), "Monte-Carlo simulation about typhoon extreme value wind characteristics in Shanghai region", *Acta Aerod. Sin.*, **27**(1), 25-31.

CC